Flow and multifragmentation of Mg-24+Al-27 at intermediate energies

Prendergast, EP; van den Brink, A; de Haas, AP; Kamermans, R; Kuijer, PG; de Laat, CTAM; Ostendorf, RW; Oti, E; Peghaire, A; Snellings, RJM

Published in:
Physical Review C

Publication date:
2000

Flow and multifragmentation of ^{24}Mg + ^{27}Al at intermediate energies

Prendergast, E. P.; Brink, A. van der; Haas, A. P. de; Kamermans, R.; Kuijer, P. G.; Laat, C. T. A. M. de; Ostendorf, R. W.; Oti, E.; Péghaire, A.; Snellings, R. J. M.

Published in:
Default journal

Publication date:
1999

Flow and multifragmentation of ^{24}Mg+^{27}Al at intermediate energies

E.P. Prendergast [a], A. van den Brink [a], A.P. de Haas [a],
R. Kamermans [a], P.G. Kuijer [a], C.T.A.M. de Laat [a],
R.W. Ostendorf [b], E. Oti [a], A. Péghaire [c], R.J.M. Snellings [d]

[a] *Universiteit Utrecht/NIKHEF, P.O.Box 80.000, 3508 TA Utrecht, The Netherlands*
[b] *KVI, Zernikelaan 25, 9747 AA Groningen, The Netherlands*
[c] *GANIL, BP 5027, 14021 Caen Cedex, France*
[d] *LBNL, 1 Cyclotron Rd, MS 50A-1148 Berkeley, CA 94720, USA*

April 6, 1999

Abstract

An elaborated investigation was done into the reaction mechanism of heavy ion collisions at intermediate energies of small nuclear systems. Experimental data measured with the Huygens detectors and IQMD simulations of ^{24}Mg+^{27}Al at 45 and 95 A MeV were analysed with respect to the impact-parameter selection, the in-plane flow and the IMF production at mid-rapidity. It was found that only the mid-central impact-parameter class could be identified effectively. The event-plane reconstruction and flow measurements were studied with IQMD and a GEANT detector simulation. This showed that the azimuthal-correlation method gives the best reconstruction. The experimentally measured in-plane flow was consistent with the balancing energy derived from literature of 114 ± 10 A MeV. The azimuthal correlations and polar-angle distributions of IMFs emitted at mid-rapidity were used to distinct between a dynamic scenario, i.e. IQMD, and a statistical scenario described by a simple decaying-source model. The IQMD simulations were in very good agreement with the experimental data and the decaying-source simulations were not, which shows that multifragmentation in these small systems is a dynamic process.

Keywords: small nuclear systems, impact parameter, flow, dynamic multifragmentation

1 Introduction

An elaborate investigation was performed into the reaction dynamics of heavy ion collisions at intermediate energies of small nuclear systems. Experimental data and IQMD simulations [1,2] of ^{24}Mg+^{27}Al at 45 and 95 AMeV provide insight into processes taking place, when the bulk of the nuclear material is small compared to the surface.
The experiments described in this paper were performed at the GANIL heavy-ion beam facility in Caen (France). GANIL provided ^{24}Mg beams which were directed onto an aluminium target foil. The measurements of the ^{24}Mg+^{27}Al collisions were performed using the Huygens detectors [3, 4]. This detector array was conceived and built at the department of subatomic physics at Utrecht University. The Huygens detector array is a 4π-detector, which allows for an *event by event* analysis of the reaction. The array was used in conjunction with a forward time-of-flight wall, the MUR [5], covering the phase space between 3° and 30° polar angle. The Huygens detectors consist of a central time projection chamber (TPC) surrounded by a plastic scintillator barrel ($11° \leq \theta_{\rm lab} \leq 78°$) and a CsI(Tl) wall (the CIW) at backward angles ($121° \leq \theta_{\rm lab} \leq 177°$). Due to experimental difficulties, the CIW could only be used as a multiplicity counter. In the mid-rapidity region, particles are detected in the TPC, which is highly symmetric in the azimuthal angle ϕ with an average accuracy of 3.1° in ϕ [4]. The polar angle resolution ($\theta_{\rm lab}$) is better than 1° at 78° and better than 0.25° at 11°. The TPC was operated at a gas pressure of 150 mbar (CF_4) leading to energy thresholds from 5 AMeV for protons to 7 AMeV for boron. Particle identification was obtained using the E vs. dE technique, with E measured in the plastics and dE measured in the gas chamber. Particles in the forward region are identified using the timing of the MUR and the energy deposition of these particles in the forward plastic scintillators of the TPC. In the MUR the polar-angle resolution is 22.5° and the

resolution of the azimuthal angle is approximately 5°. Particles with an azimuthal angle between 3° and 10° are only identified in the MUR and therefore have a threshold of approximately 20 AMeV.
For the analysis in total 4×10^6 events were used of 45 AMeV and 8×10^6 events of 95 AMeV. For the IQMD simulations the number of events are 600.000 for 45 AMeV and 800.000 for 95 AMeV. The main problem studying the collisions of these small nuclear systems is the low multiplicity. The impact-parameter selection procedure is directly related to this multiplicity, therefore, IQMD and a GEANT detector simulation were used to study the accuracy of this selection procedure. This is described in section 2. The simulations were also used to study the event-plane reconstruction efficiency and the resulting flow measurement. Four different event-plane reconstruction methods were compared and the best method was used for the analysis of the experimental data. This study and the flow measurements are described in section 3. In section 4 the IMFs emitted at mid-rapidity are studied. The azimuthal correlations and polar angle distributions are used to show that the multifragmentation process in these small nuclear systems is a dynamic process and that there is no evidence of a mid-rapidity source.

2 Impact-parameter selection

The physics of heavy-ion collisions is strongly determined by the amount of overlap between the two nuclei. This quantity is described by the impact parameter, b, which is defined as the distance between the centres of the colliding nuclei. Several methods have been proposed to measure b. These methods are generally based on the sum over one-body observables in an event, such as transverse momentum $|\mathbf{p}_\mathrm{t}|$, detected energy E_det or charged particle multiplicity N_c (see [6, 7] and references therein). Simulations with IQMD combined with the GEANT detector simulation do not show large differences in the accuracy with which b can be determined from $|\mathbf{p}_\mathrm{t}|$, E_det or N_c. For our data the charged particle multiplicity was used for the impact parameter determination. It is assumed that N_c depends monotonically on the impact parameter [7, 8]:

$$\hat{b}(N_\mathrm{c}^\mathrm{m}) = \frac{b}{b_\mathrm{max}} = \left(\int_{N_\mathrm{c}^\mathrm{m}}^{\infty} P(N_\mathrm{c}) \mathrm{d}N_\mathrm{c} \right)^{\frac{1}{2}}, \tag{1}$$

with $\hat{b}$ the impact parameter as a fraction of the maximum impact parameter, b_max, N_c^m the charged particle multiplicity for which the impact parameter is to be determined and $P(N_\mathrm{c})$ the measured probability distribution of N_c. It is assumed that the two nuclei are classical spheres, with b_max the sum of the radii (for ^{24}Mg+^{27}Al , $b_\mathrm{max} = 6.6$ fm). Fig. 1 shows $P(N_\mathrm{c})$ in the Huygens detectors for the 45 and 95 AMeV data. In the 95 AMeV data the very low multiplicities are suppressed by the trigger condition. This data set was not taken with a minimum-bias trigger, but with the requirement that either in the forward scintillators or in the sideward scintillators two or more hits were registered. The 45 AMeV data was taken with a minimum bias trigger, i.e. a single hit in one of the plastic scintillators ($\theta_{lab} > 10°$) and shows the distribution expected in heavy-ion collisions: a structureless plateau and a (near) exponential slope at higher multiplicities. Because of the small number of participating nucleons the exponential decrease starts at low multiplicities. To compensate for the trigger effects, the structureless plateau in $P(N_\mathrm{c})$ for both distributions was extended to low multiplicities. With this assumption, different impact-parameter classes can be defined using eq. 1. Three different classes are defined, peripheral for $\hat{b} > 0.7$, mid-central for $0.35 < \hat{b} < 0.7$ and central for $\hat{b} < 0.35$. For the measured multiplicity distribution this results in a definition for mid-central events for 45 AMeV of $2 < N_\mathrm{c} < 6$. For 95 AMeV mid-central is defined by $3 < N_\mathrm{c} < 7$. Higher multiplicities are central and lower multiplicities are peripheral. Because of the low multiplicity ($N_\mathrm{c} \leq 3$), peripheral events are not used in the analysis.

A similar analysis for the impact parameter can be performed on IQMD data, which is processed by the GEANT detector simulation. It should be noted that IQMD underestimates fragment formation, while proton and neutron yields are overestimated. This effect leads to an increased multiplicity for all impact parameter classes. Nevertheless, the analysis can give an indication of the accuracy of the definition of the impact-parameter classes. In fig. 2 the impact parameter is plotted of an IQMD simulation with GEANT for the three classes at 95 AMeV beam energy. The results are similar for 45 AMeV. The yield of the distributions are with a minimum-bias trigger. The mean value and the RMS of the peripheral, mid-central and central events are 4.8 ± 1.4 fm, 4.0 ± 1.5 fm and 3.3 ± 1.5 fm, respectively. The shapes of the distributions show the (in)accuracy by which the impact parameter can be determined. Therefore, these classes should merely be seen as an indication for the selected impact-parameter range. It should be noted that by selecting from these distributions events with a number of IMFs, a new implicit

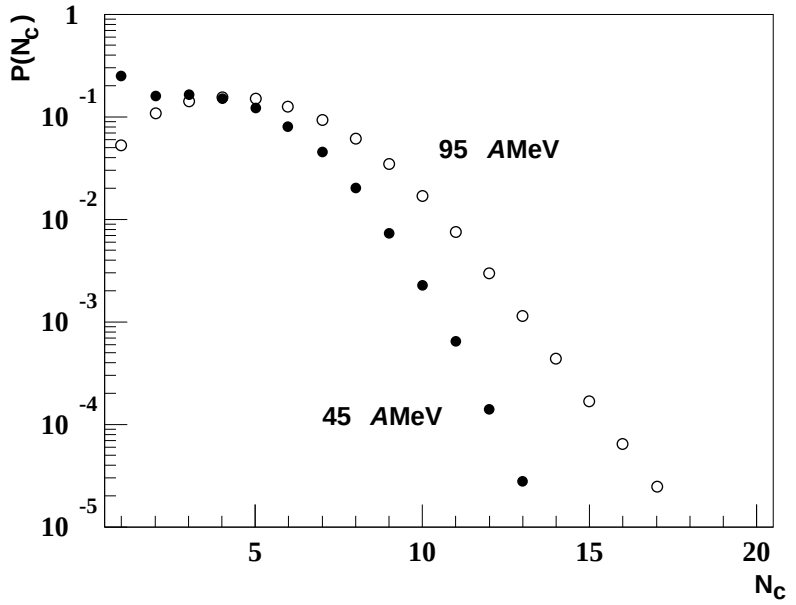

Figure 1: The measured charged particle multiplicity, $P(N_c)$ in the Huygens detectors for 45 and 95 AMeV beam energy.

impact-parameter selection is made, which will result in an even more similar event selection for the impact-parameter classes.
For the analysis only the event class 'mid-central' is used. Fig. 2 shows that the central class is heavily polluted by mid-central events. Therefore, it is not possible to draw conclusions about very central collisions. The peripheral events are, like the mid-central events, reasonably well defined. However, due to the small charged-particle multiplicity, it is not possible to do a useful analysis on these events.

3 Collective motion

The collective motion of matter in nuclear collisions is deemed to be one of the primary observables to extract information on the EOS. The attractive mean-field potential and the repulsive nucleon-nucleon interaction cause a sideward flow of fragments within the reaction plane. The magnitude of this *directed in-plane flow* is sensitive to the compressibility of nuclear matter. In the intermediate-energy region, the interest has been focussed in particular on the balancing energy, $E_{\rm bal}$, the beam energy where the two forces cancel. Although the magnitude of the directed in-plane flow was found to depend on the mass of the emitted fragment, $E_{\rm bal}$ is the same for all fragments [9]. Furthermore, both experiment and simulation show that $E_{\rm bal}$ is proportional to $A^{-1/3}$, where A is the combined mass of the colliding system [10,11]. For the study of the directed in-plane flow, the reaction plane itself has to be reconstructed. Methods to perform this reconstruction have an intrinsic error, which is inversely correlated to the number of fragments in an event. For the small system described here, IQMD and the GEANT detector-simulation program were used to study the accuracy of the event-plane reconstruction.

3.1 Event-plane reconstruction

The event plane, in experimental data, needs to be reconstructed from the observables. In simulated events, this variable is known and the effectiveness of the event-plane reconstruction can be studied. Three methods can be used to perform the reconstruction, the kinetic flow-tensor method [12], the transverse-momentum analysis [13] and the azimuthal-correlation method [14]. In this section the different methods are described briefly and the results are compared. The comparison is done using IQMD events for the ^{24}Mg+^{27}Al system at 45 and 95 AMeV before and after the simulation of the detector response.

The kinetic flow-tensor method constructs, for the determination of the reaction plane, the kinetic sphericity

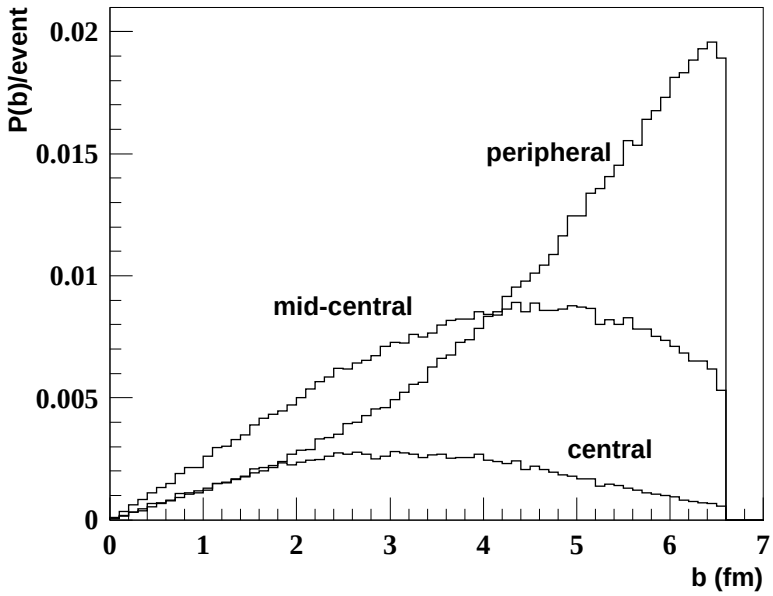

Figure 2: Impact-parameter distribution for ^{24}Mg+^{27}Al at 95 AMeV for different impact-parameter classes generated by IQMD and filtered by GEANT.

tensor F:

$$F_{ij} = \sum_{\nu=1}^{N} \omega_\nu p_{i\nu} p_{j\nu}, \tag{2}$$

with i, j running from 1 to 3, N the number of particles in an event, ω_ν a weight factor for each particle and $p_{i\nu}$ the i^{th} component of the momentum of particle ν. For the weight factor usually $\frac{1}{2m_\nu}$ is taken, with m_ν the mass of the particle, this method will be referred to as STM. For this study the method was also tested with a weight factor of 1, which will be called ST1. In heavy-ion collisions F defines a volume in space, which in general is shaped like a *cigar*. Because the tensor is symmetric, diagonalisation of F yields three real eigenvalues f_i, which are ordered such that $f_3 \lesssim f_2 < f_1$. The eigenvector associated with the largest eigenvalue, $\mathbf{e}_1$, defines the largest component of the collective flow. This component, the directed in-plane flow, spans the reaction plane with the beam direction and thus defines the reaction plane.

In the transverse-momentum analysis (TMA) only the direction of the particles perpendicular to the beam axis is considered. The reaction plane is fixed by the beam direction and the $\mathbf{Q}$ vector, which is defined by:

$$\mathbf{Q} = \sum_{\nu=1}^{N} \omega_\nu \mathbf{p}_\nu^\perp, \tag{3}$$

with the sum over all particles in an event, $\mathbf{p}_\nu^\perp$ the momentum component perpendicular to the beam axis and ω_ν the weight factor which is $+1$ for particles with $Y_\nu > 0$ and -1 for $Y_\nu < 0$. This method assumes that the flow in the forward region is associated, via momentum conservation, with flow in the opposite direction in the backward region. The weight factor assures that both directions are summed with the same sign.

STM, ST1 and TMA all explicitly use and require the directed in-plane flow for the reconstruction of the reaction plane. The azimuthal-correlation method (ACM) does not use this feature but merely requires that the particles are preferably emitted within (close to) the reaction plane. This method again only uses the momenta of the particles perpendicular to the reaction plane. The azimuthal angle of the event plane is reconstructed using a test reaction plane. The deviation, D^2, of all momenta relative to this test plane is defined in terms of the slope, a, of the projection of the test plane in the x-y plane:

$$D^2 = \sum_{\nu=1}^{N} p_{x\nu}^2 + p_{y\nu}^2 - \frac{(p_{x\nu} + p_{y\nu})^2}{1 + a^2}, \tag{4}$$

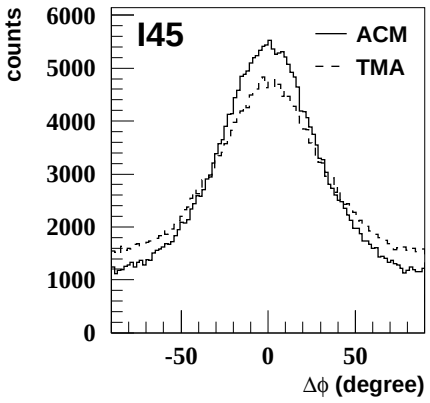

Table: RMS of $\Delta\phi$ distributions

	I45	I95	G45	G95
STM	41.5	45.1	46.2	48.4
ST1	41.5	44.4	46.8	48.5
TMA	43.0	44.8	46.7	48.4
ACM	39.8	43.4	45.8	48.2
error	0.1	0.1	0.3	0.1

Figure 3: On the left: the distributions for the difference in azimuthal angle between the reconstructed reaction plane and the real reaction plane using the transverse-momentum analysis and the azimuthal-correlation method at 45 AMeV for IQMD data. On the right: RMS of the distributions of the difference between the reconstructed event-plane and the real event plane for the four described methods, the sphericity flow-tensor method with the mass (STM) and with 1 (ST1) in the weight factor, the transverse-momentum analysis (TMA) and the azimuthal-correlation method (ACM). The last row indicates the error in the values of that column. The methods were tested at 45 and 95 AMeV before and after the detector simulation, denoted respectively with I and G. All results are for mid-central events.

with the sum being over all particles in an event and p_x, p_y the components of the momenta perpendicular to the beam. The real reaction plane is found by minimising D^2:

$$\frac{\mathrm{d}D^2}{\mathrm{d}a} = 0 \tag{5}$$

To avoid a strong auto-correlation between the angle of the particle and the angle of the reaction plane, the reconstruction of the reaction plane should be performed for each particle individually, without using the information of the particle of interest. The result of this is that for each event N different reaction planes are defined. To compensate for the momentum of the particle of interest, which is not incorporated in the analysis, all particles are boosted by a weighted velocity, $\mathbf{v}_\mathrm{b}$, related to the momentum of this particle, $\mathbf{p}_\mathrm{poi}$ [15]:

$$\mathbf{v}_\mathrm{b} = \frac{\mathbf{p}_\mathrm{poi}}{m_\mathrm{sys} - m_\mathrm{poi}}, \tag{6}$$

with m_sys the mass of the complete system and m_poi the mass of the particle of interest.

All four described methods, STM, ST1, TMA and ACM have been used to reconstruct the event plane on simulated data of mid-central events. Fig. 3 shows the results of this study. The plot on the left shows the distributions for the difference between the reconstructed reaction plane and the real reaction plane for TMA and ACM of ^{24}Mg+^{27}Al at 45 AMeV for IQMD data. All distributions show this shape and only differ in the width of the distribution. The table on the right of fig. 3 gives the RMS values of the different distributions. For all simulated data sets ACM gives the best results, although the differences, particularly after the detector simulations, are quite small. ACM has been used to reconstruct the reaction plane of the measured data. The influence of the beam energy and the detector on the distributions will be discussed shortly.

In the comparison above only the smallest angle between the calculated reaction plane and the real reaction plane was used. In fact this quantity is what can be measured experimentally. However, to do a flow analysis it is also necessary to determine the orientation of the reaction plane, i.e. whether the projectile passes the target on the left or on the right-hand side. This can not be done unambiguously. It is, however, possible to align the reaction plane for all events from the angle of the directed flow. Since it is expected that for ^{24}Mg+^{27}Al both at

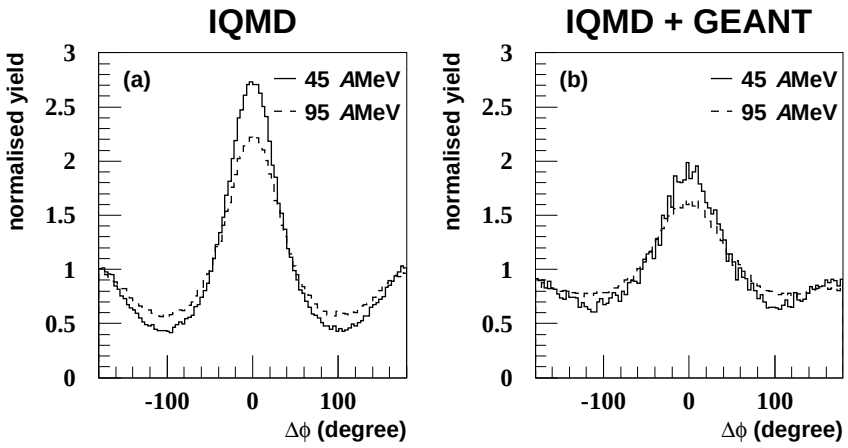

Figure 4: The angle difference between the real reaction plane and the reaction plane determined with ACM for mid-central events. On the left-hand side the results for IQMD data, on the right-hand side the results after the GEANT program was used to simulate the detector effects on the IQMD data.

45 and 95 AMeV the system experiences a negative flow, the flow is defined as beeing negative. If the calculated flow in an event is found to be positive, the reaction plane is rotated by 180°.
In fig. 4a the results of the event-plane analysis with ACM for IQMD data are shown for mid-central events. For this study all fragments with $1 \leq Z \leq 8$ were used. The 45 AMeV data shows a slightly better determination of the reaction plane than the 95 AMeV data. At 95 AMeV the number of light fragments is substantially higher than at 45 AMeV . These fragments are in general emitted more isotropically than larger fragments, which makes it more difficult to determine the reaction plane. Fig. 4b shows the results for mid-central events after the IQMD events are processed by the detector simulation. The reaction-plane determination after the detector simulation is considerably less accurate than before this simulation. This is mainly due to the reduction of the acceptance in the backward hemisphere and close to the beam. Again the 45 AMeV data shows a slightly better determination than the 95 AMeV data. Most importantly, however, from fig. 4b it can be concluded that it is possible to determine the reaction plane with the experimental data from the Huygens detectors.

3.2 Directed in-plane flow

After the study of the reaction-plane reconstruction, this information can be used to calculate the directed in-plane flow. The influence of the inaccuracy of the reaction plane on the flow must be looked at carefully to justify conclusions from the experimental data. The flow analysis will be used to show a difference in magnitude between the directed in-plane flow at 45 and 95 AMeV. With only these two data points it is not possible to extract $E_{\rm bal}$. However, this quantity has already been measured for the system ^{20}Ne+^{27}Al and has a value of 111 ± 10 AMeV [10]. Assuming that $E_{\rm bal}$ depends on the mass of the system with $A^{-1/3}$, $E_{\rm bal}$ for ^{24}Mg+^{27}Al would be 114 ± 10 AMeV. It will be shown that our measurements are in agreement with this value.

It is known that although IQMD shows directed in-plane flow, and also the disappearance of flow, the value of $E_{\rm bal}$ in IQMD is in general much larger than the experimentally measured value [16–18]. The simulations presented in this section support this for the system ^{24}Mg+^{27}Al.

To calculate the magnitude of the directed in-plane flow, the flow parameter F is defined [19]:

$$F = \frac{\mathrm{d} < p_{x^*} >}{\mathrm{d}(Y/Y_{\rm proj})}, \tag{7}$$

with p_{x^*} the component perpendicular to the beam of the projection of the momentum on the reaction plane and $Y/Y_{\rm proj}$ the rapidity in the centre of momentum frame normalised to the projectile rapidity. The value F has to be calculated around mid-rapidity, usually between $-\frac{1}{2}Y_{\rm proj}$ and $\frac{1}{2}Y_{\rm proj}$, although this domain may vary in the region where p_{x^*} vs. Y can be fitted with a straight line. Fig. 5 show the results of the flow calculations on simulated events in the mid-central impact-parameter class. In (a) and (b) the momentum projections of IQMD events on

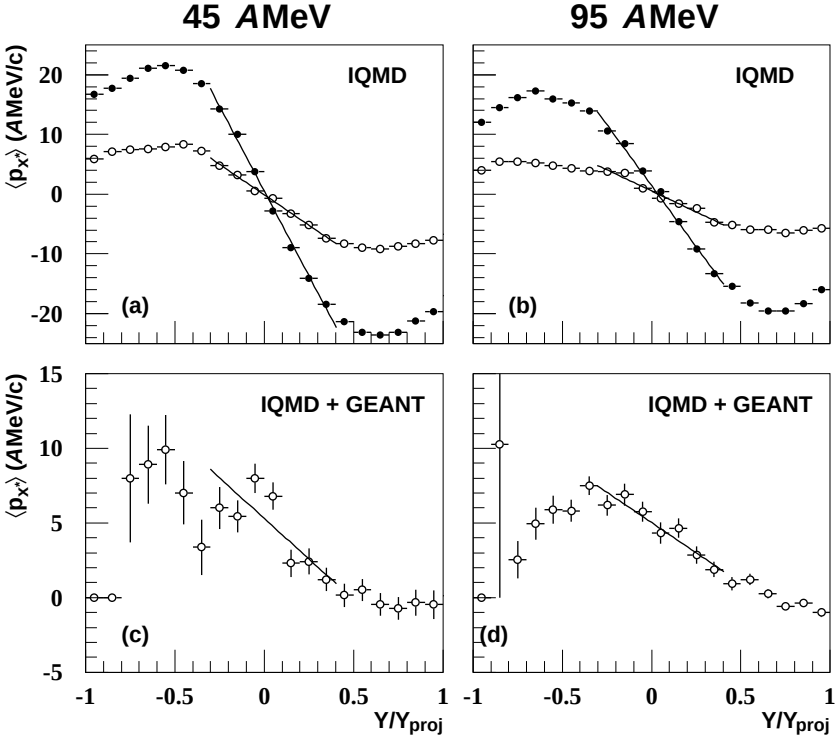

Figure 5: Average in-plane transverse momentum as a function of the rapidity normalised to the projectile rapidity. The figures on the left are for 45 AMeV data, on the right for 95 AMeV. All data is mid-central. Figures (a) and (b) are the results for IQMD events with the projection on the real reaction plane (filled circles) and on the reconstructed reaction plane with the ACM (open circles). The figures (c) and (d) show the results after the IQMD events are processed by the detector simulation, with the reconstructed reaction plane. The lines are fits of a straight line and are used to calculate the flow (see text).

the real reaction plane are shown with filled circles. These graphs show the real directed in-plane flow. The fits are also drawn in the figure, for 45 AMeV the flow is -56.5 ± 1.1 AMeV and for 95 AMeV it is -41.2 ± 1.4 AMeV. These values indicate that $E_{\rm bal}$ in IQMD is much greater than the 114 ± 10 AMeV from literature. In (a) and (b) also the momentum projections are shown for the same events, with the reconstructed reaction plane (open circles). The uncertainty in the reaction-plane reconstruction reduces the measured flow by about a factor of three, but retains the ratio between 45 and 95 AMeV. The values for the fit for these distributions are -19.9 ± 0.6 AMeV for 45 AMeV and -12.9 ± 2.1 AMeV for 95 AMeV. Figures (c) and (d) show the momentum projections after the IQMD events have been processed by the detector simulation. Again these are projections on the reconstructed event plane. The values for the flow are for 45 AMeV -12 ± 3 AMeV and for 95 AMeV -7.6 ± 2.1 AMeV. Also after the detector simulation the ratio between the data sets are retained (within the error). Fig. 5c and 5d show that directed in-plane flow can be determined with the Huygens detectors using the procedures described above.

Fig. 6 gives the results of the directed in-plane flow measurements of the Huygens data of mid-central events. On the left-hand side the results of the momentum projection on the reconstructed reaction plane is shown for all IMFs. Similar to the IQMD data after the GEANT simulations, the measurements show a positive offset of $<p_{x^*}>$, which is due to the acceptance of the Huygens detectors. The simulations have shown that, despite this offset, the flow value F can still be used to measure directed in-plane flow. Clearly the flow is substantially reduced at 95 AMeV as compared to 45 AMeV. The flow analysis was also performed for the different Z-classes individually, the results of which are presented in the table on the right-hand side of fig. 6. Heavy fragments show a larger flow than light fragments, but they all result in a similar $E_{\rm bal}$, as is readily reported in literature (e.g. [9]). The errors in the results include the statistical error and the systematic error due to the selection of the fit area. The most important systematic error which is not taken into account, is the error in the event-plane reconstruction at small flow angles, as is the case at 95 AMeV. Because the directed in-plane flow is used to reconstruct the reaction

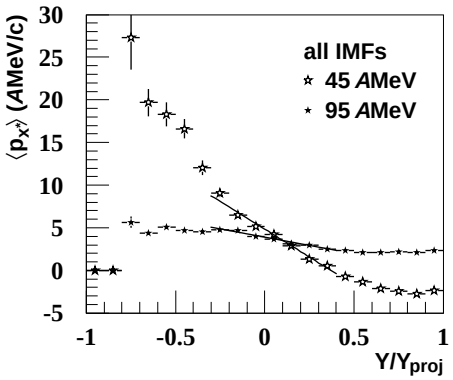

Table: flow values in AMeV/c

	45 AMeV	95 AMeV
all IMFs	−12.9(1.1)	−3.2(1.2)
$Z = 2$	−10.4(1.5)	−3.3(1.4)
Z = 3-4	−19.9(1.7)	−4.7(2.5)
Z = 5-8	−33(4)	−6.3(3.7)

Figure 6: On the left, as in fig. 5 for measured data. The results of the fit are shown in the table on the right. Also the results for the different Z-classes are shown.

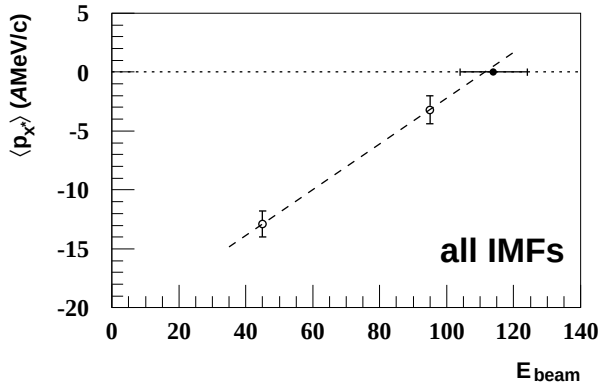

Figure 7: Measured directed in-plane flow data (open circles) compared to the value derived from literature (filled circle). The line connects the two measured data points and serves to guide the eye.

plane, the accuracy of the reconstruction depends on the magnitude of the flow. It is not possible to study this with IQMD, because the directed in-plane flow at 95 AMeV is still too large compared to the experimental results. The accuracy of the event-plane reconstruction could be calculated by splitting the event into two sub-events and then calculating the event plane for both sub-events. However, the multiplicity in our data-set is too small for such an analysis. This effect is, therefore, not be corrected for. In general a linear fit is used to determine $E_{\rm bal}$ from the measured flow values (e.g. [9, 10]). Fig. 7 shows the measured flow values (open circles) for ^{24}Mg+^{27}Al and the value derived from [10] (filled circle). The measured data points are in agreement with this value for $E_{\rm bal}$ of 114 ± 10 AMeV.

4 IMFs at mid-rapidity

The origin of IMF emission in heavy-ion reactions is a heavily debated subject in the field of intermediate-energy heavy-ion physics [20–31]. The nature of the production process will depend on the mass and energy of the colliding systems. In this section measurements of the azimuthal correlations and polar-angle distributions are described for the ^{24}Mg+^{27}Al system at 45 and 95 AMeV. As shown before, the latter energy is close to the balancing energy of approximately 110 AMeV [10]. Here it will be shown that the combination of these two methods shows that IMF production for these small systems is a dynamic process, with no evidence of the formation of a mid-rapidity source.

4.1 Azimuthal correlations

Azimuthal correlations are considered to be a powerful tool to probe the dynamics of heavy-ion reactions, free from uncertainties in the reconstruction of the reaction plane [19, 32–34]. In this method the angular correlations of fragments emitted in the mid-rapidity region of the reaction are studied. The azimuthal-correlation method does not require an *event by event* reconstruction of the reaction plane and minimises other systematic uncertainties associated with detector acceptance and efficiency. Azimuthal correlations have been used to study many of the features of heavy-ion collisions, such as directed and rotational flow [19,33,35–37], balancing energy [32] and impact parameter [38].

The azimuthal-correlation method uses the angular difference in the azimuth, $\Delta\phi$, of different fragments to study the reaction dynamics. It makes use of the azimuthal-correlation function, which is defined as the ratio of the azimuthal angle differences of correlated fragments, $N_{\mathrm{cor}}(\Delta\phi)$ and the angle differences of uncorrelated fragments, $N_{\mathrm{uncor}}(\Delta\phi)$:

$$C(\Delta\phi) = \frac{N_{\mathrm{cor}}(\Delta\phi)}{N_{\mathrm{uncor}}(\Delta\phi)}. \tag{8}$$

The correlated angles are from fragments within one event. Uncorrelated fragments are generated by mixing tracks from different events. Events are mixed which are of the same impact-parameter class and have the same fragment multiplicity. These generated mixed events are corrected for the detector granularity, so two tracks are not identified by the same detector module. Real events are also corrected for this to ensure that events are processed similarly in the two (corrected and uncorrected) distributions. From this point on the term 'mixed events' will be used to indicate events consisting of uncorrelated fragments.

If particles are emitted independently, the azimuthal-correlation function is described by the auto-correlation function of the single-particle distribution:

$$C(\Delta\phi) = \int_0^{2\pi} P(\phi)P(\phi + \Delta\phi)\mathrm{d}\phi, \tag{9}$$

With $P(\phi)$ the distribution of independently emitted fragments. Empirically it has been shown that the fragment distribution is described by a second-order Legendre polynomial [38, 39]:

$$P(\phi) \propto 1 + a_1 \cos(\phi) + a_2 \cos(2\phi). \tag{10}$$

The value a_1 can be related to the *in plane* flow and the value a_2 is attributed to other directed motion, either *squeeze out*, if $a_2 < 0$ or rotational effects if $a_2 > 0$. If eq. 10 is substituted in eq. 9, the azimuthal-correlation function can be calculated for independently emitted fragments:

$$C(\Delta\phi) \propto \lambda_1 \cos(\Delta\phi) + \lambda_2 \cos(2\Delta\phi), \tag{11}$$

where the relationship between a_i and λ_i is given by:

$$\lambda_i = \tfrac{1}{2}a_i^2, \tag{12}$$

which again associates the first term in eq. 11 with directed flow and the second term with other collective motion, usually rotational effects, as derived in [36].

The azimuthal-correlation function will be used in our analysis to exclude the scenario of independently emitted fragments from a mid-rapidity source described above. Furthermore, the polar-angle distributions will be studied to distinguish between fragments emitted from a small decaying source and a dynamic production process described by IQMD. The analysis is restricted to the mid-rapidity region and the mid-central impact-parameter class. The peripheral class has a multiplicity which is too low to justify any conclusions and are excluded from the analysis. Central events show essentially the same azimuthal distributions as mid-central events. Small differences in these distributions can not be seen independently from the overall higher multiplicity of selected fragments. Because the number of fragments is used to select the centrality of the events, no conclusions can be drawn from this difference.

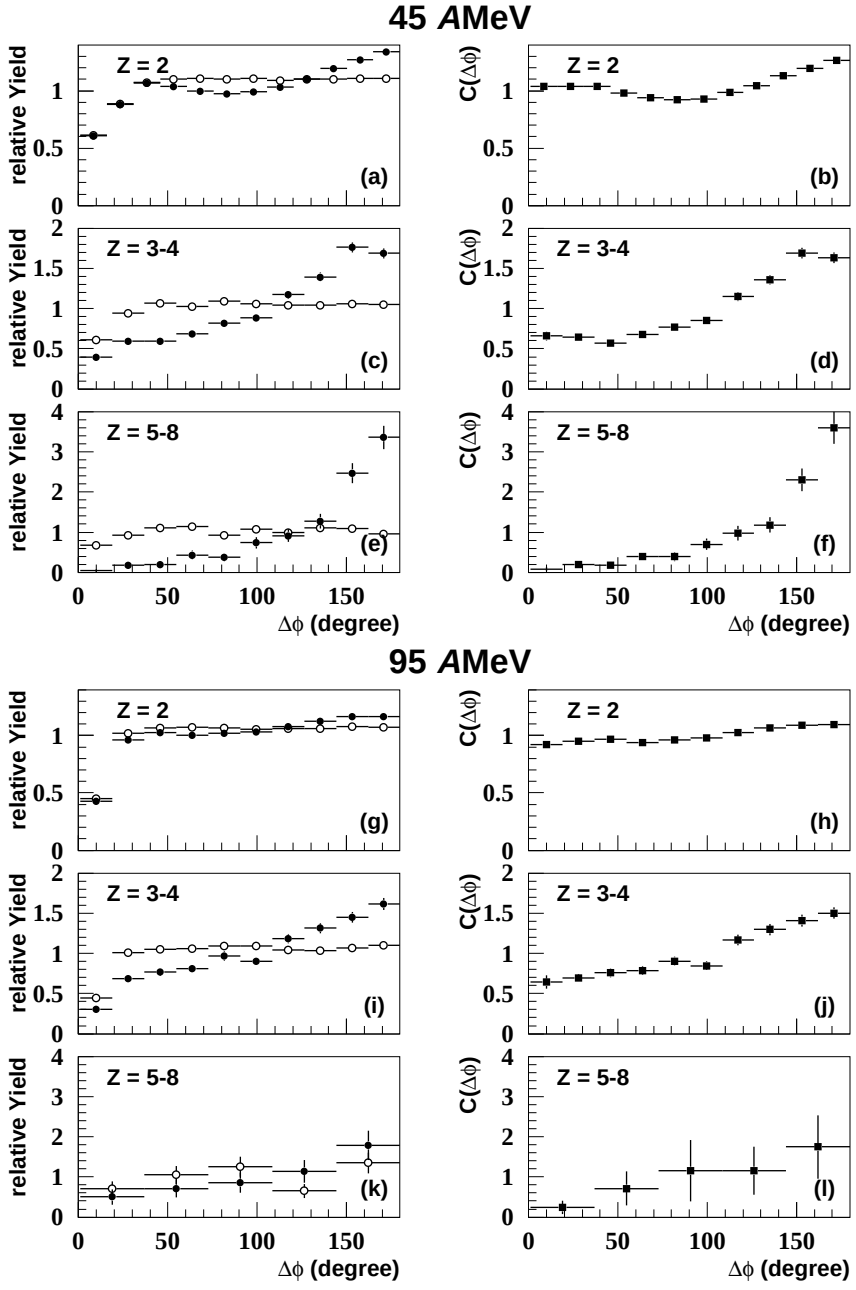

Figure 8: Azimuthal correlations for different fragments and beam energies for mid-central events. The left column shows the raw-data correlations (filled circles) and the correlations for mixed events (open circles). The right column gives the ratio of the two: the azimuthal-correlation function. All plots are normalised to the integrated area of the distributions.

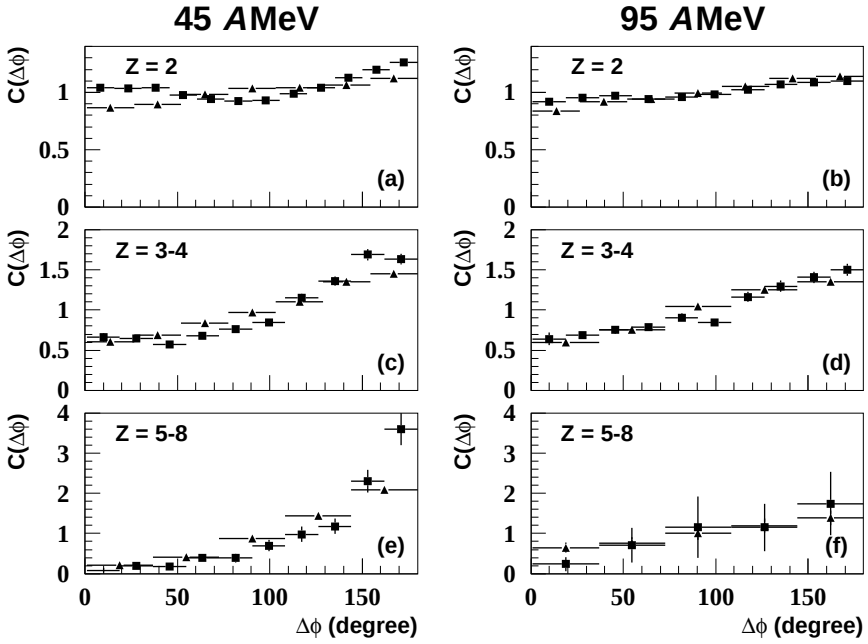

Figure 9: Azimuthal correlations of the experimental data (filled squares) and IQMD events (filled triangles). All events are mid-central, the fragment charge is indicated in the top-left corner of each plot.

4.2 Results

In fig. 8 the azimuthal correlations for the experimental data at mid-rapidity with impact-parameter class mid-central are shown. The analysis is restricted to particles which are identified in the Huygens set-up between 10° and 78° polar angle, in the laboratory system. All figures are normalised with respect to the integrated surface of the distributions. The top six figures are for the 45 AMeV data, the bottom six are for the 95 AMeV data. On the left-hand side the correlated azimuthal distributions are shown with filled circles and the azimuthal distributions of mixed events are shown with open circles. On the right the ratio of the two (see eq. 8) shows the azimuthal-correlation function with filled squares. The fragments which are selected in the different figures are indicated in the top-left corner. The azimuthal-correlation functions at the two energies are for each Z-class quite similar, however, it was shown in section 3.2 that the directed in-plane flow at 45 AMeV is substantially larger than at 95 AMeV. From this it can be concluded that the azimuthal correlations are insensitive to directed in-plane flow. Clearly, all distributions show an enhancement at 180°, which increases with fragment mass. Only the $Z = 2$ data at 45 AMeV shows a small increase at 0°. A description of the distributions with eq. 11 will yield a negative value for λ_1, using eq. 12 this will lead to an imaginary value for a_1. This clearly shows that these distributions can not be explained by independently emitted fragments.

Two models have been used to investigate the reaction mechanism for ^{24}Mg+^{27}Al at 45 and 95 AMeV. Firstly, the IQMD model gives a dynamic picture of the heavy-ion collision, without the inclusion of an equilibrated system at mid-rapidity. Secondly, because the maximum at 180° in the azimuthal distribution function could be due to momentum conservation of a small decaying source [34, 40, 41], a simple static-source model was used to describe the measured distributions.

In fig. 9 the azimuthal distributions of the experimental data are compared to the IQMD results. Comparison of the azimuthal distribution functions of IQMD events before and after the detector simulations showed no difference. To enhance the statistics, the azimuthal distributions of IQMD without the GEANT detector simulation are shown. Only the $Z = 2$ results are different for IQMD and the experimental data. This is due to a different production process for $Z = 2$ than the IMFs, which is not incorporated in IQMD. All other distributions of the experimental data and IQMD are in good agreement.

To describe the decaying mid-rapidity source, a simple participant/spectator scenario was assumed. Events

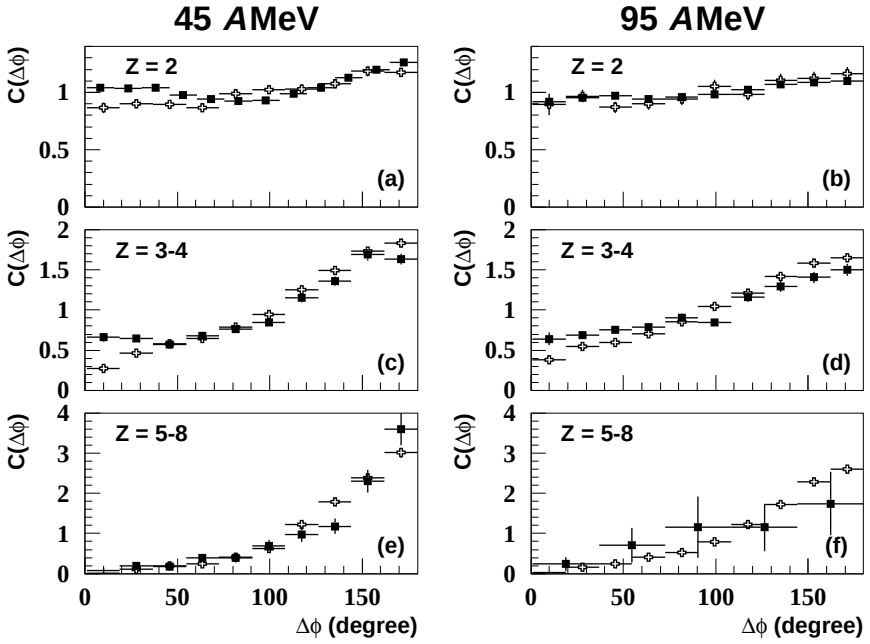

Figure 10: Azimuthal correlations of the experimental data (filled squares) and of the static-source events filtered by GEANT (open crosses). The experimental data are mid-central, for details on the static-source data, see text. The fragment charge is indicated in the top-left corner of each plot.

were generated using a model describing a small static source at mid-rapidity undergoing prompt multifragmentation [42]. In this model the Coulomb interaction is neglected and the multifragmentation process is governed by phase space. The source size, the excitation energy and the decay mode are input parameters. The excitation energy for the source was taken to be the average centre-of-mass energy per nucleon, i.e. 11 AMeV and 23 AMeV for beam energies of 45 AMeV and 95 AMeV, respectively. The distributions from this static-source model were also processed by the GEANT detector simulation. The source size was used as a parameter to fit the azimuthal distributions of the static-source model to the data. This fit was performed for each fragment-class individually and has an accuracy of approximately 10%. In fig. 10 the resulting azimuthal distributions (open crosses) are compared to the data (filled squares). The source sizes do not depend on the beam energy. They do, however, depend on the mass of the emitted IMFs. For the $Z = 2$ data the mass of the source is 32 amu, for Z = 3-4 the mass is 36 amu and for Z = 5-8 the mass is 40 amu. The decay mode has very little influence on the distributions. Simulations for Z = 3-4 decaying in one $Z = 3$, one $Z = 4$ and several small fragments show essentially the same azimuthal distributions as a three particle decay mode. The decaying static-source distributions are in agreement with the experimental data, although the levelling of the experimental data (and the IQMD data) at small angles is not reproduced. Therefore, the static-source model and IQMD give an equally good description of the measured azimuthal distributions.

Although it is not possible to distinguish the two described models by studying the azimuthal correlations, the polar-angle distributions should be able to make a distinction [43]. Any decaying source at mid-rapidity will have a maximum in these distributions at 90°, whereas the polar-angle distributions of IQMD show a minimum at 90° flanked by two maxima [43, 44]. It was shown that these maxima in IQMD are remnants of the target and the projectile and are therefore called target-like and projectile-like [44]. This is a fundamental difference between the two models; an equilibrated decaying source has lost by definition all information about its initial state, whereas IQMD shows a strong initial-final state correlation. Fig. 11 shows the polar-angle distribution at mid-rapidity for the different fragments at the two beam energies. On the left-hand side the IQMD results after GEANT (grey line) are compared to the measured distributions (black line), on the right-hand side the measured distributions (black line) are shown with the static-source results (grey line).
For 45 AMeV the IQMD results nicely describe the measured data. For Z = 3-4, fig. 11c shows for both IQMD and the measured data target and projectile-like maxima. Fig. 11d shows the same distributions for the measurement and the static-source model. These two figures clearly show that the experiment and IQMD are in agreement and

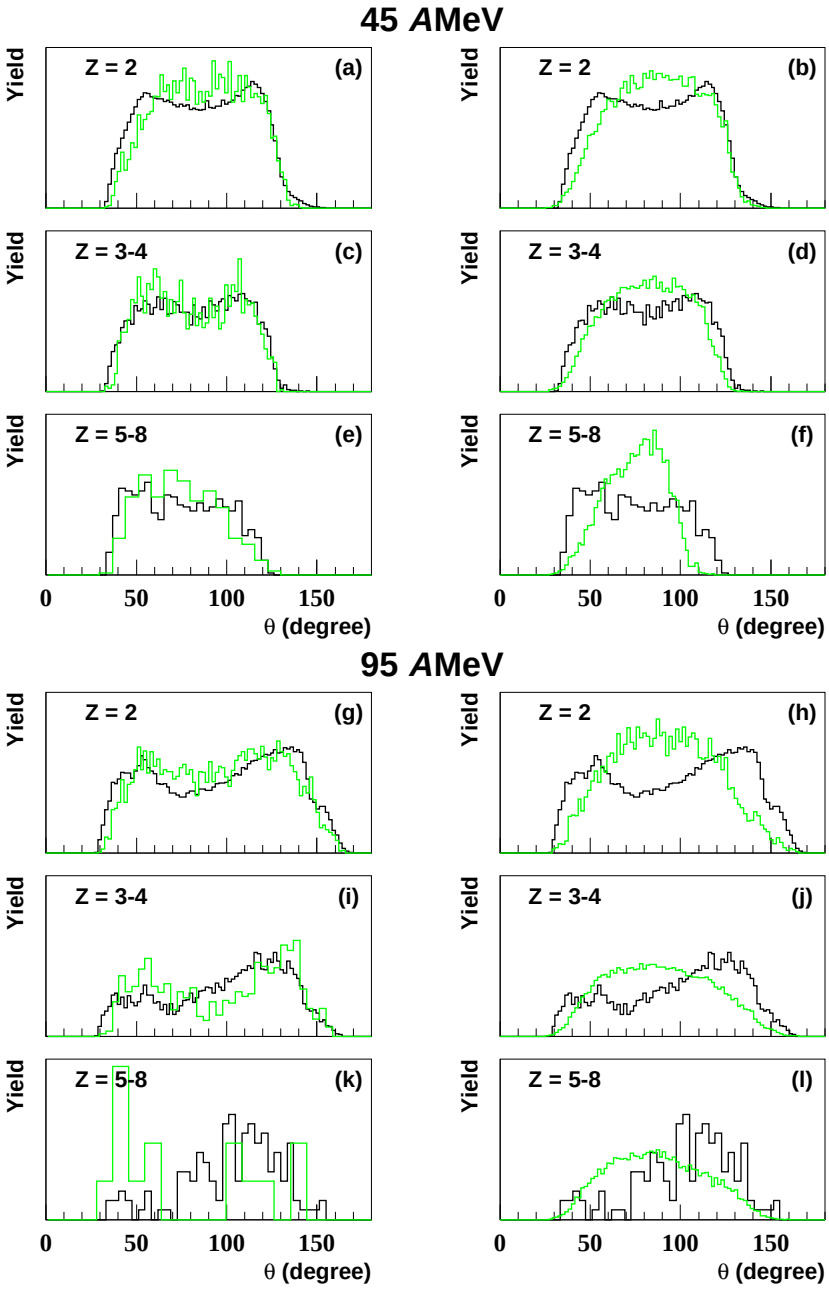

Figure 11: Polar-angle distributions for the experimental data (black lines) and on the left-hand side IQMD data after GEANT (grey lines) and on the right the static-source data (grey lines). The fragment charge is indicated in the top-left corner of each plot.

that the static-source model fails to describe the measurement. In fact, as was already stated, any decaying-source model will always show a peak in the polar-angle distribution at 90°, which is contradicted by the measurement. For heavy fragments, fig. 11d and fig. 11e show that the measurement is in agreement with IQMD and is different from the static-source model. For these fragments the projectile-like and target-like maxima fall outside the experimentally accessible domain. The figures 11a and 11b for the $Z = 2$ distributions show no significant difference between IQMD and the static-source model. The data, however, seems to indicate target-like and projectile-like maxima. As in the azimuthal-correlation function this difference between the experimental data and IQMD is probably due to a different production process for $Z = 2$. The 95 AMeV distributions show essentially the same results as the 45 AMeV distributions. The experiment is well described by IQMD and the static-source model fails to describe the data. For $Z = 2$ the data in fig. 11g show definite target-like and projectile-like maxima in both the measured data and IQMD. The static-source model in fig. 11h shows a maximum where both other distributions show a minimum. This is also the case in fig. 11j for Z = 3-4. The enhancement in fig. 11i and fig. 11j for the measured data at small angles is caused by misidentified α-particles in the gas chamber. Despite this, the data still shows target-like and projectile-like maxima, similar to the IQMD distribution. Statistics do not allow for a comparison of the Z = 5-8 data, for completeness they are shown in figures 11k and 11l.
From the polar-angle distributions a clear distinction can be made between a decaying-source scenario and a purely dynamic process as described by IQMD.

4.3 Discussion

In the previous section the azimuthal-distribution function of mid-rapidity particles in conjunction with the polar-angle distributions showed that the IMF emission in nuclear mid-central collisions of ^{24}Mg+^{27}Al at 45 AMeV and 95 AMeV is governed by dynamic processes with no experimental evidence of a mid-rapidity source. The maxima in the azimuthal distributions were shown to be due to the correlations between target-like and projectile-like fragments.
It was found that the azimuthal correlations of mid-rapidity particles for both energies are quite similar, whereas the measured directed in-plane flow is substantially higher at 45 AMeV than at 95 AMeV and are consistent with an E_{bal} of 114 ± 10 AMeV. This shows that the azimuthal correlations are insensitive to the directed in-plane flow. The azimuthal-correlation functions of mid-rapidity particles in the aforementioned reaction exhibit pronounced maxima at 180°. This maximum increases with fragment size and its existence is not influenced by the beam energy. The measured azimuthal distributions can not be caused by a single mid-rapidity source emitting particles independently [33,35–37], because the distribution can not be described using the auto-correlation function (eq. 9). Coulomb repulsion [36, 45] is also not responsible for the maxima in the azimuthal distributions [43]. Therefore, the maxima at 180° can only be explained if the emitted particles are strongly correlated [32]. Momentum conservation of a small decaying source can be responsible for this maximum [34, 40, 41]. Therefore, a model of a small static decaying source was used to fit to the data. More elaborate models, such as a hot fast-spinning source, a multifragmentation source or a statistical-decay source [40, 41] can also be used. However, all these models yield a maximum in the polar-angle distribution at 90°. The GEANT simulations show that the Huygens detector is sensitive to this maximum. However, the measured data does not show a maximum at this angle, but instead shows a minimum, flanked by a projectile-like and a target-like maximum, which are nicely described by the IQMD results.
A superposition of three sources, a mid-rapidity source, a target-like source and a projectile-like source [46], or a two-source model with only the latter two [47], is in our case not necessary because the measured data is in good agreement with IQMD simulations. Because IQMD is a dynamic model, this agreement in itself is evidence for a reaction governed by dynamic processes.
It can be stated that the nuclei of the small system studied in this thesis are not able to form a compound system. Literature shows that by increasing the size of one of the nuclei, the azimuthal distributions start to show a more symmetric shape [34,41]. This could indicate that pressure from the surrounding nuclear matter forces the creation of a compound system. However, as was shown above, very different scenarios can lead to a similar azimuthal-correlation function. The azimuthal-correlation function should, therefore, not be taken as conclusive evidence of any scenario.

acknowledgments

We would like to thank the colleagues at GANIL for their valuable help and the LPC for making the 'MUR' available. We would also like to thank C. Hartnack for providing the IQMD code. This work was performed as part of the 'Stichting voor Fundamenteel Onderzoek der Materie' (FOM) with financial support from the 'Nederlandse Organisatie voor Wetenschappelijk Onderzoek' (NWO).

References

[1] J. Aichelin, Phys. Rep. 202 (1991) 233.

[2] C. Hartnack, Ph.D. thesis, GSI-Report 93-05 (1993), ISBN 0171-45446.

[3] T.M.V. Bootsma *et al.*, Nucl. Instr. and Meth. A349 (1994) 204.

[4] E.P. Prendergast, Ph.D. Thesis, Universiteit Utrecht (1999), ISBN 90-393-1830-1.

[5] G.Bizard *et al.*, Nucl. Instr. and Meth A244 (1986) 483.

[6] C.A. Ogilvie *et al.*, Phys. Rev. C40 (1989) 654.

[7] L. Phair *et al.*, Nucl. Phys. A548 (1992) 489.

[8] C. Cavata *et al.*, Phys. Rev. C42 (1990) 1760.

[9] C.A. Ogilvie *et al.*, Phys. Rev. C42 (1990) 10.

[10] G.D. Westfall *et al.*, Phys. Rev. Let. 71 (1993) 1986.

[11] V. de la Mota *et al.*, Phys. Rev. C46 (1992) 677.

[12] M. Gyulassy, K.A. Frankel and H. Stöcker, Phys. Let. B110 (1982) 185.

[13] P. Danielewicz and G. Odyniec, Phys. Let. B157 (1985) 146.

[14] W.K. Wilson *et al.*, Phys. Rev. C45 (1992) 738.

[15] C.A. Ogilvie *et al.*, Phys. Rev. C40 (1989) 2592.

[16] S. Soff *et al.*, Phys. Rev. C51 (1995) 3320.

[17] R.J.M. Snelling, Ph.D. thesis, Utrecht University (1998), ISBN 90-393-1634-1.

[18] C. Liewen, Z. Fengshou, and J. Genming, Phys. Rev. C58 (1998) 2283.

[19] J.C. Angélique *et al.*, Nucl. Phys. A614 (1997) 261.

[20] A.S. Botvina and D.H.E. Gross, Phys. Rev. C58 (1998) 23.

[21] J. Tõke and W.U. Schröder, preprint cern-th/9807066 (1998).

[22] A.S. Botvina and D.H.E. Gross, preprint CERN, nucl-th/9808004 (1998).

[23] L. Phair *et al.*, Phys. Rev. Let. 75 (1995) 213.

[24] M. D'Agostino *et al.*, Phys. Let. B371 (1996) 175.

[25] N. Marie *et al.*, Phys. Let. B391 (1997) 15.

[26] L. Beaulieu *et al.*, Phys. Rev. Let. 81 (1998) 770.

[27] L. Phair *et al.*, preprint LBNL-41893 (1998), sub. Phys. Rev. C.

[28] J. Tõke *et al.*, Phys. Rev. Let. 77 (1996) 3514.

[29] J. Tõke *et al.*, Phys. Rev. C56 (1997) 1683.

[30] M.F. Rivet *et al.*, preprint GANIL P9815 (1998), acc. Phys. Let. B.

[31] O. Tirel *et al.*, preprint GANIL P9826 (1998).

[32] A. Buta *et al.*, Nucl. Phys. A584 (1995) 397.

[33] R.A. Lacey *et al.*, Phys. Rev. Let. 70 (1993) 1224.

[34] C.B. Chitwood *et al.*, Phys. Rev. C34 (1989) 858.

[35] S. Wang *et al.*, Phys. Rev. C44 (1991) 1091.

[36] L. Phair *et al.*, Phys. Rev. Let. 77 (1996) 822.

[37] W.Q. Shen *et al.*, Phys. Rev. C57 (1998) 1508.

[38] W.Q. Shen *et al.*, Nucl. Phys. A551 (1993) 333.

[39] M. Demoulins *et al.*, Phys. Let. B241 (1990) 476.

[40] T. Ethvignot *et al.*, Phys. Rev. C47 (1993) 2099.

[41] T. Ethvignot *et al.*, Phys. Rev. C48 (1993) 618.

[42] F. James, CERN report 68-15 (1968).

[43] R.J.M. Snelling *et al.*, Phys. Let. B426 (1998) 263.

[44] P.-B. Gossiaux and J. Aichelin, Phys. Rev. C56 (1997) 2109.

[45] T.M. Hamilton *et al.*, Phys. Rev. C53 (1996) 53.

[46] T. Lefort *et al.*, Cont. to the XXXVI Int. winter meeting on Nucl. Phys. (1998), Bormio (Italy).

[47] M. Germain *et al.*, Internal Report SUBATECH 97-09, (1997).